energies

MDPI

Article

Application of Sulfated Tin (IV) Oxide Solid Superacid Catalyst to Partial Coupling Reaction of α-Pinene to Produce Less Viscous High-Density Fuel

Seong-Min Cho [1], Chang-Young Hong [2], Se-Yeong Park [3], Da-Song Lee [1], June-Ho Choi [1], Bonwook Koo [4] and In-Gyu Choi [1,5,6,*]

1 Department of Forest Sciences, College of Agriculture and Life Sciences, Seoul National University, Seoul 08826, Korea; csmin93@snu.ac.kr (S.-M.C.); ds0429@snu.ac.kr (D.-S.L.); jhchoi1990@snu.ac.kr (J.-H.C.)
2 Department of Forest Biomaterials, College of Natural Resources, North Carolina State University, Raleigh, NC 27695, USA; chong6@ncsu.edu
3 Department of Forest Biomaterials Engineering, College of Forest and Environment Science, Kangwon National University, Chuncheon 24341, Korea; parksy319@kangwon.jac.kr
4 Intelligent & Sustainable Materials R&D Group, Korea Institute of Industrial Technology (KITECH), Cheonan 31056, Korea; bkoo@kitech.re.kr
5 Research Institute of Agriculture and Life Sciences, College of Agriculture and Life Sciences, Seoul National University, Seoul 08826, Korea
6 Institutes of Green-Bio Science and Technology, Seoul National University, Pyeongchang 25354, Korea
* Correspondence: cingyu@snu.ac.kr; Tel.: +82-2-880-4785

Received: 19 April 2019; Accepted: 16 May 2019; Published: 18 May 2019

Abstract: Brønsted acid-catalyzed reactions of α-pinene have been studied because of their ability to produce various types of fragrance molecules. Beyond this application, dimeric hydrocarbon products produced from coupling reactions of α-pinene have been suggested as renewable high-density fuel molecules. In this context, this paper presents the application of a sulfated tin(IV) oxide catalyst for the partial coupling reaction of α-pinene from turpentine. Brønsted acid sites inherent in this solid superacid catalyst calcined at 550 °C successfully catalyzed the reaction, giving the largest yield of dimeric products (49.6%) at 120 °C over a reaction time of 4 h. Given that the low-temperature viscosity of the mentioned dimeric products is too high for their use as a fuel in transportation engines, lowering the viscosity is an important avenue of study. Therefore, our partial coupling reaction of α-pinene provides a possible solution as a considerable amount of the isomers of α-pinene still remained after the reaction, which reduces the low-temperature viscosity. On the basis of a comparison of the reaction products, a plausible mechanism for the reaction involving coinstantaneous isomerization and coupling reaction of α-pinene was elucidated.

Keywords: solid superacid catalyst; sulfated tin(IV) oxide; α-pinene partial coupling; renewable high-density fuel

1. Introduction

Turpentine, one of the most widely produced plant-derived secondary metabolites, is a mixture of monoterpenes. It is made up mainly of α-pinene and its isomers, such as β-pinene and camphene. Depending on the production method, it is categorized as gum turpentine (produced from oleoresins of conifers), wood turpentine (produced from aged pine stumps), sulfate turpentine (produced by the kraft pulping process), and sulfite turpentine (produced by the sulfite pulping process) [1]. Concerns about fossil fuel depletion and environmental destruction urge us to develop alternative energy resources. In this regard, turpentine, in which C10 hydrocarbons form major components, has been

reported as a potential candidate for providing biofuel blends for fueling both spark ignition engines and compression ignition engines [2–5].

A coupling reaction by which C20 hydrocarbons can be synthesized from renewable α-pinene has been devised for ramjet propulsion [6–8], but not for conventional jet fuels. This is because the relatively high carbon number of these compared to that of petroleum-derived fuels tremendously increases their low-temperature viscosity, which limits the suitability of using dimeric products alone for transport fuel [9]. Thus, the partial coupling of monoterpene hydrocarbons was suggested as one possible solution [10]. This agrees with the results reported by Harvey et al., who suggested blending dimeric products with monoterpene hydrocarbons such as α-pinene, thereby resolving the viscosity problem of dimeric products [6].

Coupling of monoterpene hydrocarbons has been studied using various types of heterogeneous acid catalysts, such as Nafion, Nafion SAC-13, montmorillonite K10, Al-incorporated MCM-41, Pd-Al-incorporated MCM-41, phosphotungstic acid supported on MCM-41, phosphotungstic acid supported on SiO_2, Zeolite Hβ, and silica-alumina aerosol [6–8,11–14]. Given that the isomerization of monoterpene hydrocarbons is usually attributed to Brønsted acid activity and that Brønsted acids can also assist in their coupling reactions undertaken in harsh conditions, it has been thought that the catalytic activities of the above catalysts are caused by Brønsted acid sites and the role of Lewis acid sites is less significant.

Herein, we used sulfated tin(IV) oxide (SO_4^{2-}/SnO_2) as a solid superacid catalyst to carry out partial coupling of α-pinene for the production of less viscous high-density fuel molecules. SO_4^{2-}/SnO_2 catalysts have been used in various types of organic reactions, such as dehydration of sorbitol and xylose to isosorbide and furfural, respectively, esterification of free fatty acids, the Penchmann condensation reaction, and deprotection of silyl ether groups [15–19]. Successive chemical precipitation and immersion in diluted sulfuric acid yielded this catalyst from tin chloride pentahydrate in a facile procedure. In this study, the catalyst successfully furnished dimeric products from α-pinene with its isomers in solventless conditions. On the basis of the results, a plausible mechanism for the isomerization and coupling reaction, in which Brønsted acid catalysis plays a central role, was also suggested. To our knowledge, no attempt has been made so far to propose a mechanism considering both reactions together.

2. Materials and Methods

2.1. Catalyst Preparation

To prepare the catalysts, tin oxide powder obtained from tin (IV) chloride pentahydrate ($SnCl_4{\cdot}5H_2O$) by chemical precipitation, followed by drying, was used as a precursor. Briefly, a transparent 0.1 M tin chloride solution was prepared by dissolving $SnCl_4{\cdot}5H_2O$ in distilled water. To hydrolyze the tin chloride complex, a 28 wt% aqueous ammonia solution was added dropwise under vigorous stirring. The addition was stopped when the pH of the solution reached approx. 8. After a precipitate was separated from clear supernatant liquid, thorough washing was carried out with a 4 wt% ammonium acetate solution by centrifugation. The white product was then dried in an oven at 105 °C for 24 h and ground into a fine powder. The prepared tin oxide (SnO_2) powder (10 g) was placed in a round flask containing 3 g of sulfuric acid diluted with 20 mL of distilled water. After sufficient stirring at 80 °C, water was removed in vacuo and sulfuric acid-treated SnO_2 was dried and stored in an oven at 65 °C. This precatalyst was dried further at 120 °C for 12 h, followed by calcination at 450, 550, 600, and 650 °C for 4 h.

2.2. Catalyst Characterization

To understand the properties of the prepared catalysts and elucidate their catalytic activity, we conducted X-ray diffraction (XRD) analysis, field-emission scanning electron microscopy (FE-SEM), thermogravimetric analysis (TGA), and temperature-programmed desorption of ammonia (NH_3-TPD).

The XRD patterns of the catalysts were collected to compare the crystal structures. The surface morphology of the catalysts was investigated using FE-SEM. Energy dispersive X-ray spectroscopy (EDS) and elemental mapping were also performed as part of the SEM investigation. To study the thermal properties of the catalysts, TGA was carried out. NH_3-TPD was performed to characterize the improvement in the catalyst acidity. The detailed analysis conditions are described in the Supplementary Materials.

2.3. Catalytic Tests

In a typical experiment, turpentine (5 g), tridecane (2 g, GC internal standard), and catalysts (0.1 g) were added without any solvent to a 50 mL glass flask equipped with a magnetic Teflon-coated stirrer and a reflux condenser. The reactor was then loaded on a preheated aluminum heating block and stirred vigorously. Upon completion of the reaction, the reactor was removed from the heating block and immediately cooled to room temperature using a cold-water bath. After cooling, the crude reaction mixture was diluted with n-hexane (100 mL) and filtered over a Celite pad. To estimate the product composition by the internal standard method, a diluted reaction mixture was analyzed using a gas chromatograph (7890B) equipped with a DB-5ms column (30 m × 250 μm, 0.25 μm thickness), a mass spectrometer detector (5977A), and a flame ionization detector (Agilent Technologies, Santa Clara, CA, USA). The yield of the products and the conversion rate of α-pinene were calculated using the following equations:

$$\text{Yield of product } i\ (\%) = \frac{\text{Weight of product } i}{\text{Weight of crude reaction mixture}} \times 100, \quad (1)$$

$$\text{Conversion rate of } \alpha-\text{pinene}\ (\%) = \frac{\text{Consumed weight of } \alpha-\text{pinene}}{\text{Initial weight of } \alpha-\text{pinene}} \times 100. \quad (2)$$

3. Results and Discussion

3.1. Catalyst Characteristics

3.1.1. Catalyst Surface Morphology

To investigate the surface morphological properties of intact tin oxide (SnO_2) and sulfated tin oxide (SO_4^{2-}/SnO_2), field emission-scanning electron microscopy (FE-SEM) observation was carried out. The SEM images in Figure 1a,b show that intact SnO_2 has a rough surface, whereas SO_4^{2-}/SnO_2 exhibits a smooth one because, although both surfaces consist of globular nanoparticles, the size of the nanoparticles in SO_4^{2-}/SnO_2 was much smaller than that of the nanoparticles in intact SnO_2. Energy dispersive spectroscopy (EDS) analysis confirmed the presence of sulfur-containing groups on the surface of SO_4^{2-}/SnO_2 (Figure S1a–d). In addition, elemental mapping images clearly show a uniform distribution of sulfur atoms on the surface (Figure 1c and Figure S1e).

3.1.2. Catalyst Crystal Structure

The crystal structures of tin oxide (SnO_2) and sulfated tin oxide (SO_4^{2-}/SnO_2) calcined at 550 °C was characterized using powder X-ray diffraction, as shown in Figure 2. There were obvious differences in the diffraction peaks for the species. The diffractogram of intact SnO_2 shows a good match to the ICDD powder diffraction file of cassiterite SnO_2 (PDF 00-041-1445), which means that it has a tetragonal crystal structure similar to that of cassiterite SnO_2 (P42/mnm space group). Major diffraction peaks observed at $2\theta = 27°$, 34°, and 52° could be indexed to the (110), (101), and (211) planes of cassiterite SnO_2, respectively. Immersion in diluted sulfuric acid before calcination significantly influenced the crystal structure. Even though the characteristic diffraction peaks of cassiterite SnO_2 were detected in the diffractogram of SO_4^{2-}/SnO_2, the intensities of the peaks decreased significantly and their breadth broadened considerably. Because this weakening and broadening denotes diminished crystallinity

and crystallite size [16,20], Figure 2 suggests an amorphous structure and small-sized crystallites of SO_4^{2-}/SnO_2. In accordance with the results presented in previous studies related to sulfated metal oxides such as SnO_2 and ZrO_2, sulfate groups on the surface of sulfuric acid immersed SnO_2 seem to hamper both aggregation and crystallization themselves during calcination [17,21,22]. This result also coincides with the FE-SEM images shown in Figure 1, which shows the difference in the size of globular nanoparticles making up the surfaces.

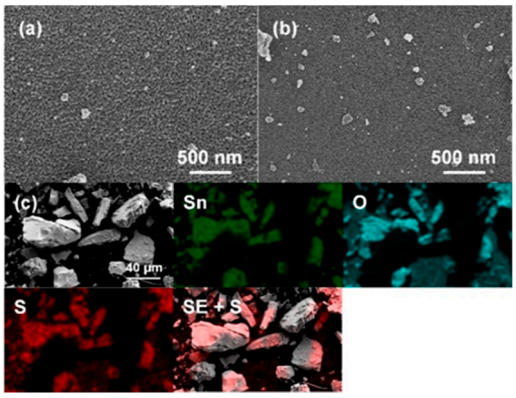

Figure 1. Field-emission scanning electron microscopy (FE-SEM) images of the surface of (**a**) intact SnO_2; and (**b**) SO_4^{2-}/SnO_2; (**c**) SEM-energy dispersive X-ray spectroscopy (EDS) elemental mapping images of SO_4^{2-}/SnO_2. The samples were prepared by calcination at 550 °C for 4 h. In the overlay image of SEM and sulfur atom mapping, the gray color represents an area in shadow or surface facing away from the EDS detector.

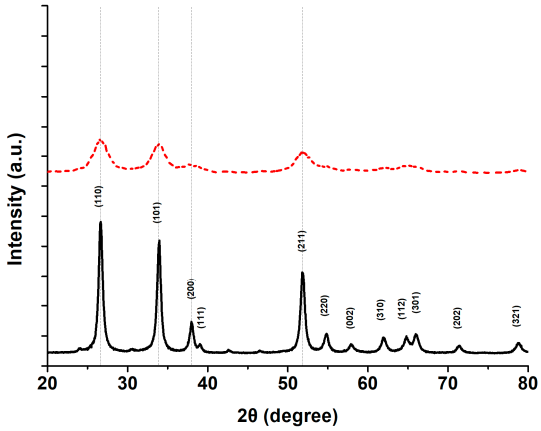

Figure 2. X-ray diffraction patterns of intact SnO_2 (black line) and SO_4^{2-}/SnO_2 (red dashed line). The samples were calcined at 550 °C. On the basis of the ICDD powder diffraction file (PDF 00-041-1445), the peaks were indexed as tetragonal crystal structure as cassiterite SnO_2 ($P4_2/mnm$ space group).

3.1.3. Catalyst Thermostability

The catalyst was designed to be applied to the coupling of α-pinene under somewhat harsh reaction conditions (≥100 °C). Our query was whether the catalytic activity over sulfated tin oxide (SO_4^{2-}/SnO_2) could be sustained during the reaction. Because sulfate groups introduced on the surface of the SO_4^{2-}/SnO_2 support by immersion in diluted sulfuric acid are responsible for the catalytic activity [23], the thermal decomposition behavior of sulfate groups was investigated by thermogravimetric analysis (TGA). Figure S2 shows the TGA graph of intact SnO_2 and SO_4^{2-}/SnO_2 calcined at 550 °C. SO_4^{2-}/SnO_2 displayed two distinguishable weight loss sections, whereas intact SnO_2 presented gradual weight reduction throughout the temperature range. The weight reduction of intact SnO_2 and the first weight loss of SO_4^{2-}/SnO_2 from 120 to 550 °C can be explained by the desorption

of chemisorbed water molecules and dehydroxylation on the surface of the SnO_2 support [20,22]. The difference between the extents of the weight reduction experienced by them may be attributed to the differences in the surface functional groups, especially sulfate groups, on which water can interact [23]. In addition, significant weight loss was observed at temperatures higher than 600 °C in the case of SO_4^{2-}/SnO_2, which is attributed to the decomposition of sulfate groups on the surface of the SnO_2 support [20,22].

3.1.4. Catalyst Acidity

To qualitatively evaluate the acidities of the intact tin oxide (SnO_2) and sulfated tin oxide (SO_4^{2-}/SnO_2) catalysts, we carried out temperature programmed desorption of ammonia (NH_3-TPD). The TPD profiles of desorbed ammonia clearly show an improvement in the acid strength of the catalysts when SnO_2 was immersed in diluted sulfuric acid before calcination (Figure 3a). Peak deconvolution can help us interpret the meaning of the overlapped peaks. As can be seen in Figure 3b, the profile of intact SnO_2 calcined at 550 °C consisted mainly of two peaks centered at approx. 372 °C (dark yellow) and 513 °C (dark cyan), which are attributed to weak and strong chemisorption of ammonia. On the other hand, the SO_4^{2-}/SnO_2 calcined at 550 °C had four kinds of acid sites which present four peaks centered at approx. 240 °C (magenta), 353 °C (blue), 531 °C (purple), and 736 °C (orange) (Figure 3c). In particular, the strongest acid sites were attributed to the desorption of ammonia from sulfate groups on the surface of SO_4^{2-}/SnO_2 [24]. This interpretation coincided with the TGA results for SO_4^{2-}/SnO_2 shown in Figure S2, which displays a significant weight loss at temperatures higher than 600 °C due to the decomposition of sulfate groups on the surface. In addition to the obvious differences in the peak number and overall peak intensities in the TPD profiles, the amount of NH_3-uptake by the catalysts also suggests that immersion in diluted sulfuric acid generates much more acid sites than those developed in intact SnO_2 (Table 1).

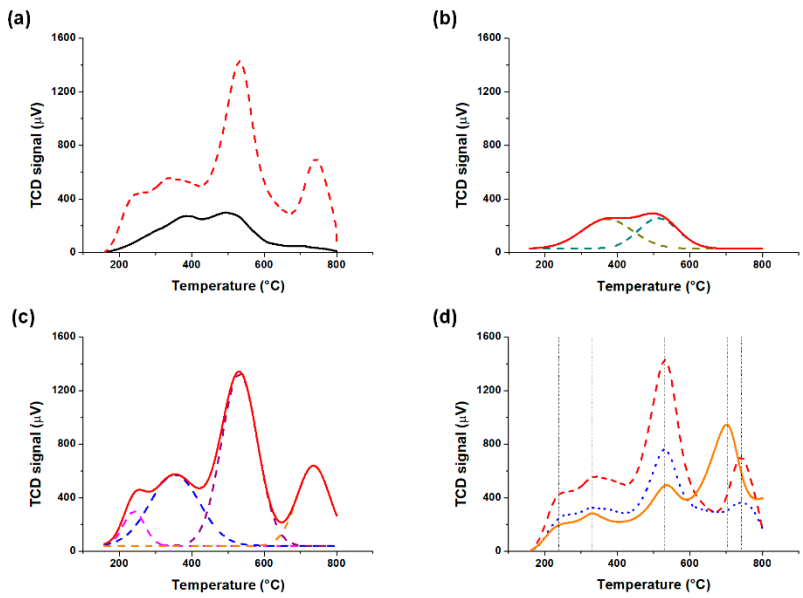

Figure 3. (**a**) Temperature programmed desorption of ammonia (NH_3–TPD) profiles of intact SnO_2 (black line) and SO_4^{2-}/SnO_2 (red dashed line); (**b**–**c**) Deconvolution of overlapped peaks in the profiles. The samples were prepared by calcination at 550 °C for 4 h; (**d**) NH_3–TPD profiles of SO_4^{2-}/SnO_2 calcined at 550 °C (red dashed line), 600 °C (blue dotted line), and 650 °C (orange line).

The effect of the calcination temperature on the acidity of the sulfated catalyst was evaluated based on the amount of NH_3 uptake (Table 1). Generally, increasing the calcination temperature reduces the total acid sites of sulfated or phosphated solid acid catalysts [25,26]. Our results coincide with those reported. However, one difference was found above the 600 °C calcination temperature, with a new

peak centered at approx. 696 °C appearing and the disappearance of the peak centered at approx. 736 °C in the TPD profiles (Figure 3d).

Table 1. NH_3 uptake of intact SnO_2 and SO_4^{2-}/SnO_2 calcined at different temperatures.

Catalyst	Intact SnO_2 [1]	SO_4^{2-}/SnO_2			
		450 °C [2]	550 °C	600 °C	650 °C
NH_3 uptake (μmol g^{-1})	171.1 [3]	1161.8	760.2	400.1	425.0

[1] Intact SnO_2 was calcined at 550 °C. [2] Calcination temperature. [3] Calculated based on the NH_3–TPD results.

3.2. Catalytic Tests and Reaction Mechanism

3.2.1. Effect of Catalyst Calcination Temperature on Partial Coupling Reaction of α-Pinene

When it comes to preparing a sulfated metal oxide catalyst using sulfuric acid treatment, a sintering process is important because the promotion of sulfate groups on the surface of metal oxide occurs during calcination and the acid sites generated by these sulfate groups offer the essential catalytic activity [23]. Figure 4 shows stark differences in the effect of the calcination temperature on the catalytic activity of sulfated tin oxide (SO_4^{2-}/SnO_2). The yield of dimeric products from α-pinene (**1**) was the largest for the catalyst calcined at 550 °C (48.9 ± 1.2%), while almost no conversion to dimeric products and significantly lowered production were observed below and above this temperature, respectively. When we tried to correlate the yield of dimeric products with the amount of the total acid sites of catalysts, unlike previous papers [25,26], there was a large discrepancy in the calcination temperature range from 450 to 550 °C (Table 1 and Figure 4). Although the catalyst calcined at 450 °C showed the highest NH_3 uptake, it was not able to furnish dimeric products at all. Since a large amount of sulfuric acid can hinder the growth of SnO_2 crystals (Figure 2), thereby leading to poor promotion of sulfate groups on the surface of SO_4^{2-}/SnO_2, the negligible catalytic activity of catalyst calcined at 450 °C (α-pinene conversion rate <20%) was attributed to sulfuric acid remaining in large quantities during the calcination process. Zhang et al. reported that increasing the calcination temperature from 150 to 550 °C made sulfate groups of SO_4^{2-}/CeO_2 transition from surface sulfate states to bulk sulfate states; the catalyst mainly possessing sulfate groups as surface sulfate states worked well in catalytic reduction of NO by NH_3. According to the Raman spectra in which only the catalyst calcined at 550 °C presented the peaks denoting bulk sulfate states, this transition seems to occur abruptly when the calcination temperature increased from 450 °C to 550 °C [27]. In this respect, the discrepancy between the yield of dimeric products and the amount of the total acid sites of catalysts can be understood by considering that the catalyst possessing sulfate groups as bulk sulfate states is effective in the coupling reaction of α-pinene. On the other hand, calcination temperatures higher than 550 °C caused significant decomposition of sulfuric acid and even sulfate groups on the surface of SO_4^{2-}/SnO_2 (Figure S2). Therefore, when the same amount of sulfuric acid was treated, a much higher calcination temperature made the catalyst lose sulfate groups. In this regard, the less effective catalytic activity of catalysts calcined at 600 and 650 °C can be understood. Finally, to compare the effect of the promotion of sulfate groups on the catalytic activity, we conducted the reaction with intact SnO_2 calcined at 550 °C, which showed negligible α-pinene conversion (data not shown).

In contrast to dimeric products, catalysts prepared at higher calcination temperatures (600 and 650 °C) more readily furnished camphene (**6**) from α-pinene (**1**) and the catalyst calcined at 550 °C also yielded a considerable amount of compound **6** (Figure 4). In other words, the conversion to compound **6** competed with the production of dimeric products from compound **1**, and once formed, compound **6** was thought to be indifferent to the homocoupling reaction with these catalysts. This is supported by the fact that several catalysts lack the ability to catalyze homocoupling of compound **6** to form dimeric hydrocarbon products [11].

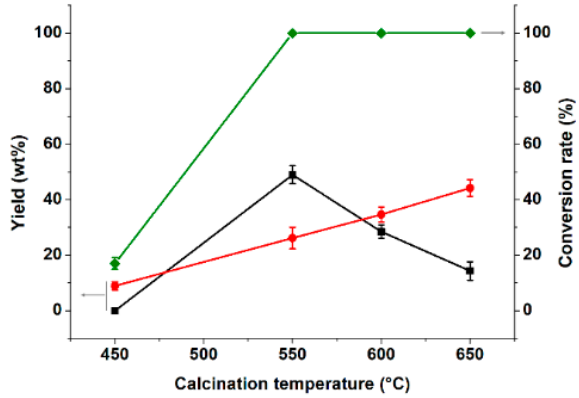

Figure 4. Effect of catalyst calcination temperature on the yields of dimeric products (■) and camphene (●) and the conversion rate of α-pinene (♦). All the other reaction conditions were maintained for 3 h at 120 °C.

3.2.2. Effect of Reaction Time and Temperature on Partial Coupling Reaction of α-Pinene

To investigate the effects of reaction time and temperature on the yield of dimeric products, we selected the sulfated tin oxide (SO_4^{2-}/SnO_2) catalyst calcined at 550 °C based on the results shown in Figure 4. As one can see in Figure 5, the conversion of α-pinene (**1**) was almost 100 ± 0% only after 30 min except for the reaction at 100 °C. This consumption furnished dimeric products almost entirely at the beginning of the reaction (Figure 5a). The additional increase in the yield continued up to 3 h at all reaction temperatures. A quite interesting feature was that after 3 h, there was no significant difference among the yields of dimeric products at 100, 110, and 130 °C, although the increase in the yield of dimeric products during the reaction was the highest at 100 °C (from 13.6 ± 3.2% to 45.0 ± 0.7%). A significant difference after 3 h was only observed at 120 °C, which produced the highest yield of all (48.9 ± 1.2%). However, when we carried out the reaction further in these conditions, there was a poor improvement (from 48.9 ± 1.2% to 49.6 ± 0.7%). In other words, only around half of compound **1** yielded dimeric products and therefore our catalyst did not seem suitable for the coupling reaction. However, considering the low-temperature viscosity of dimeric products [9], this partial coupling will be even more appropriate for fuel applications [10].

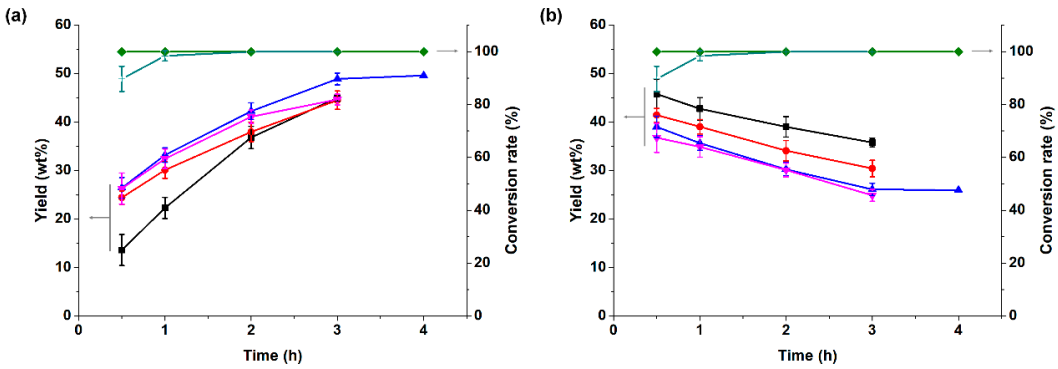

Figure 5. Effect of reaction time and temperature on the yields of (**a**) dimeric products and (**b**) camphene: (■) for 100 °C; (●) for 110 °C; (▲) for 120 °C; (▼) for 130 °C; (■) for α-pinene conversion rate except for 100 °C condition; (+) for α-pinene conversion rate at 100 °C condition. The used catalyst was prepared by calcination at 550 °C for 4 h.

Figure 5b shows that the yields of camphene (**6**) decreased depending on the reaction temperature and time. Given compound **6** seems to be less reactive to homocoupling with our catalyst, its decrease during the reaction time implies the possibility of heterocoupling of compound **6** with other species, even including dimeric products. Because such heterocoupling can consume dimeric products and

furnish oligomeric products, reaction temperatures higher than 120 °C produced a lower yield of dimeric products.

In order to investigate why the yields of both dimeric products and camphene did not show major changes after 3 h, we conducted a reusable test of the catalyst to prove whether or not the deactivation of the catalyst occurred during the reaction. Unfortunately, the used catalyst did not furnish dimeric products (data not shown). We thought that this was due to the sludge generated by the condensation of various substrates covering the acid sites of the catalyst. An interesting result was that thorough washing with acetone also cannot restore the activity of the used catalyst, but rather eliminated the activity. This is because the acetone washing removed not only the sludge but also the sulfate groups of bulk sulfate states [27]. As mentioned before, sulfate groups as bulk sulfate states of catalysts seem to have key role in the coupling of α-pinene (**1**).

3.2.3. Mechanism of Isomerization of α-Pinene over Sulfated Tin Oxide

Finally, the mechanism of isomerization and coupling reaction of α-pinene (**1**) over the sulfated tin oxide (SO_4^{2-}/SnO_2) catalyst was considered. The generally accepted mechanism of acid-catalyzed isomerization of compound **1** includes two distinct pathways [28]: ring enlargement rearrangement (path **A**), wherein tri- or bicyclic compounds are produced; and ring opening rearrangement (path **B**), in which monocyclic compounds are formed (Scheme 1). Both pathways are initiated by protonation of olefin in compound **1** generating pinanyl cation (**2**). If the highly strained 4-membered ring in carbocation **2** suffers from ring enlargement by Wagner–Meerwein rearrangement, bornanyl cation (**3**) is formed. This carbocation **3** can produce tricyclene (**4**) via direct deprotonation or camphene (**6**) via deprotonation of isocamphanyl cation (**5**) resulting from 1,2-sigmatropic rearrangement of carbocation **3**. Alternatively, carbocation **2** can be stabilized by the opening of the four-membered ring, which results in *p*-mentha-1-en-8-yl cation (**7**). In light of the similarity in structure and stability between carbocation **7** and *p*-mentha-1-en-4-yl cation (**8**), the 1,2-hydride shift between them is considered reversible. These carbocations (**7** and **8**) can be deprotonated to furnish monocyclic compounds (**9**–**12**).

In the above mechanism, the selectivities of camphene (**6**) from path **A** and limonene (**9**) from path **B** are of interest, and it is undeniable that the selectivities depend on what catalyst is used. Because compound **9** can further isomerize to other monocyclic compounds, catalysts showing the higher (but not by much) selectivity for compound **6** compared to that for compound **9** have been reported more commonly. Kitano et al. reported isomerization of α-pinene (**1**) over an Al_2O_3-supported MoO_3 catalyst, which presented a slightly higher selectivity toward compound **6** than for compound **9,** although the conversion of compound **1** was not good enough [29]. SiO_2- or MCM-41-supported $H_3PW_{12}O_{40}$ and MSU-S BEA or Y catalysts showed over 90% conversion of compound **1** and a slightly higher selectivity for compound **6** [12,30,31]. Furthermore, very powerful catalysts such as Fe^{3+}-exchanged clinoptilolite, sulfated zirconia, SBA-15 supported TiO_2, and sulfuric acid-treated montmorillonite clay have been suggested for the production of compound **6** with prominent selectivity [28,32–35]. However, catalysts that showed the higher selectivity for compound **9** compared to compound **6** have been reported much less frequently. Yamamoto et al. developed a SiO_2-supported Pr_2O_3 catalyst, which showed very high selectivity for compound **9** although the conversion of compound **1** was notably low [36]. In addition to this catalyst, a SiO_2-supported $AlCl_3$ catalyst showed higher (but not by much) selectivity for compound **9** with the varying conversion of compound **1**. In this study, SO_4^{2-}/SnO_2 showed much higher selectivity for compound **6** than for compound **9** with 100% conversion of compound **1** (Figure 5b and Figure S3). This tendency can be justified by the difference between compounds **6** and **9** in reactivity for further isomerization as mentioned previously. It has also been reported that Al-MCM-41 lacks the ability to catalyze homocoupling of compound **6** formed by the isomerization of compound **1** [11]. Given the significant amount of compound **6** still remaining after the coupling reaction was over, not only further isomerization but also homocoupling of compound **6** seems to be difficult with our catalyst, as mentioned in the previous section.

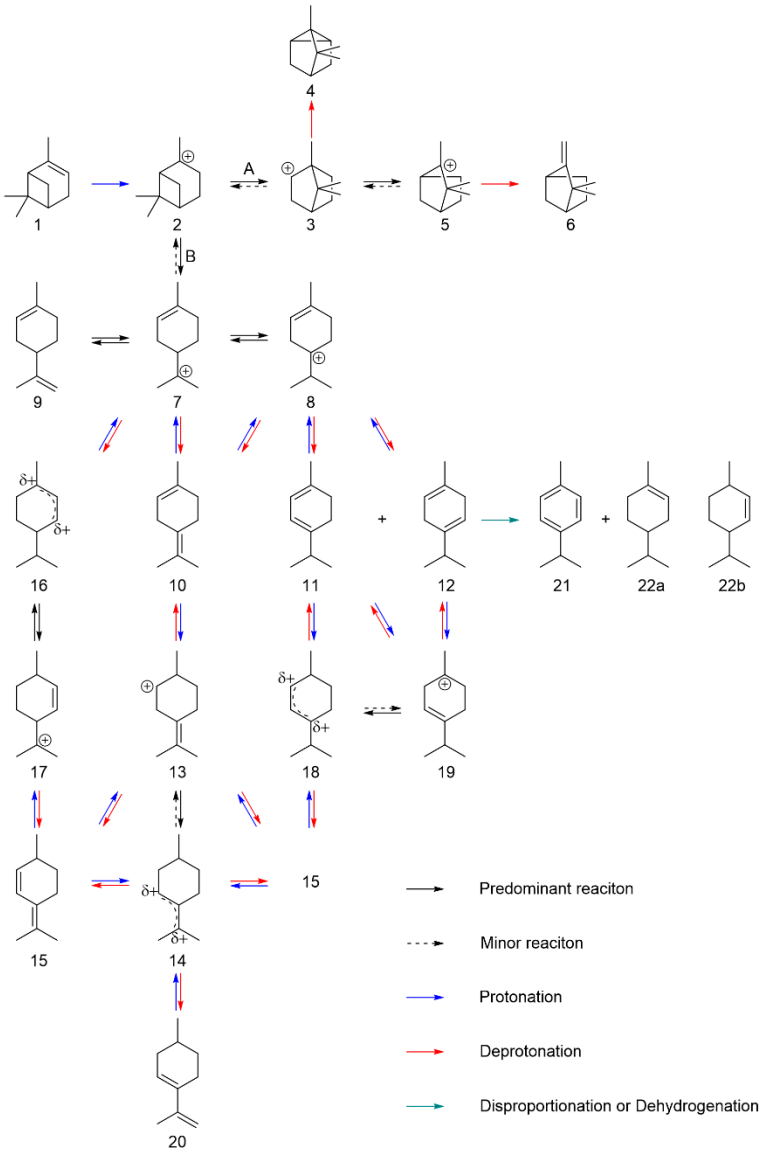

Scheme 1. Plausible mechanism of isomerization of α-pinene over sulfated tin oxide catalyst: α-pinene (**1**); pinanyl cation (**2**); bornanyl cation (**3**); tricyclene (**4**); isocamphanyl cation (**5**); camphene (**6**); *p*-mentha-1-en-8-yl cation (**7**); *p*-mentha-1-en-4-yl cation (**8**); limonene (**9**); terpinolene (**10**); α-terpinene (**11**); γ-terpinene (**12**); *p*-mentha-4(8)-en-2-yl cation (**13**); allylic carbocation I (**14**); isoterpinolene (**15**); allylic carbocation II (**16**); *p*-mentha-2-en-8-yl cation (**17**); allylic carbocation III (**18**); *p*-mentha-3-en-1-yl cation (**19**); *p*-mentha-3,8-diene (**20**); *p*-cymene (**21**); *p*-menthene isomers (**22a**–**c**).

In some papers, isoterpinolene (**15**) has been also suggested as a co-product. One plausible mechanism for the formation of compound **15** starts from protonation of terpinolene (**10**), resulting in *p*-mentha-4(8)-en-2-yl cation (**13**) [28]. Not only can direct deprotonation of carbocation **13** generate compound **15**, but also deprotonation of allylic carbocation I (**14**) resulting from carbocation **13** via 1,2-hydride shift can do the same. However, this suggestion has been controversial considering various isoterpinolene/terpinolene concentration ratios, either higher or lower than 1 [37]. A second possible mechanism is initiated by protonation of α-terpinene (**11**) or γ-terpinene (**12**), which gives allylic carbocation III (**18**) and *p*-mentha-3-en-1-yl cation (**19**). This proposal was supported by Salacinski's results which showed the chemical equilibria of *p*-menthadiene species under sulfuric acid at 67 °C [38]. When compound **11** or **12** reacted under this condition as a sole starting material, the chemical equilibrium consisted of only compounds **11**, **12**, **15**, and a small amount of *p*-mentha-3,8-diene

(**20**), where stabilization by the formation of a conjugated diene was considered the driving force. In addition, the author described reaction coordinate diagrams with allylic carbocations (**14** and **18**) as reaction intermediates. The presence of compound **20** in our results, even though the quantity of it was relatively small, also seems to indicate this mechanism. Additionally, the successive transformation of *p*-mentha-1-en-8-yl cation (**7**) into allylic carbocation II (**16**) and *p*-mentha-2-en-8-yl cation (**14**) via 1,3- and 1,5-hydride shifts, respectively, was suggested as the other possible route for the formation of compound **15** [39]. Behr and Wintzer also reported that compound **15** was formed as a major side product when the hydroaminomethylation of compound **9** was carried out with a $[Rh(cod)Cl]_2$/TPPTS catalyst [40], which means that compound **9** can be a linchpin when it comes to the production of compound **15**. As seen in Figure S3, the yield of compound **15** seems to follow the same trend as that of **9** along the reaction time. This also suggests that the third suggested pathway chiefly occurs during the isomerization of α-pinene (**1**) in the case of our catalyst.

In addition to the above-isomerized products, *p*-cymene (**21**) and *p*-menthene isomers (**22a**–**c**) were detected in the reaction mixture. The simultaneous formation of compounds **21** and **22a**–**c** can be explained by disproportionation between α-terpinene (**11**) and γ-terpinene (**12**) [6,11]. Moreover, dehydrogenation of compounds **11** and **12** was suggested to justify the production of compound **21** with the generation of hydrogen gas [41,42]. Given the para position of methyl and isopropyl groups therein, compound **21** was generally reported as the target product not only when α-pinene (**1**) was used in neat form [41,43] or as a major constituent of crude sulfate turpentine [44], but also when limonene (**9**) was used as a sole starting material [42,45]. The concentration of compound **21** in the reaction mixture gradually increased with reaction time (Figure S3). This is because it did not participate in further reactions, including both the isomerization and coupling reaction in our catalytic system [7,12].

3.2.4. Mechanism of Coupling of α-Pinene over Sulfated Tin Oxide

The lack of knowledge about the molecular structure of dimeric products obtained from monoterpene is attributed to the simultaneous homo- and heterocoupling that occurs for the starting materials and the isomers therein [6,11,12]. Furthermore, it being hard to isolate only one dimeric product from a product mixture, the study of their molecular structure has proven difficult. These phenomena were also observed in our results; although the reaction started with α-pinene (**1**) as a sole substance, besides isomerization, a variety of dimeric products were concurrently produced (Figure S4). Nevertheless, some reports have suggested several possible molecular structures without an understanding of the complicated reaction system [7,11,46].

Acid-catalyzed coupling reactions of monoterpene hydrocarbons generally involve three steps: first, the protonation of olefin in monoterpene giving carbocations; next, the attack of olefin (nucleophile) in another monoterpene on the previous carbocation (electrophile) furnishing a dimeric carbocation with the formation of a new C–C bond between the nucleophile and the electrophile; and, finally, the deprotonation of this carbocation giving dimeric products. Of course, dimeric carbocations formed by nucleophilic attack on monomeric carbocations, or even by the re-protonation of dimeric products, can suffer from isomerization and further coupling reactions, which is one reason for the complexity of the reaction mechanism. In addition to coupling reactions that involve protonation/deprotonation, the Diels–Alder reaction between monoterpenes, especially α-terpinene (**11**), has also been suggested as a possible mechanism for the coupling reaction of monoterpenes [47].

In light of the results obtained for a reaction at a relatively low temperature (100 °C, Figure S3a), although the concentration of α-pinene (**1**) in the reaction mixture precipitously decreased with reaction time, considering almost all of the dimeric products were yielded in just 30 min, compound dimeric structure (**PD1**). We can also imagine that further isomerization of this possible dimeric product gives, for example, **PD1a** and **PD1b** via ring enlargement and ring opening, respectively.

The isomers of α-pinene (**1**), such as camphene (**6**), limonene (**9**), terpinolene (**10**), α-terpinene (**11**), γ-terpinene (**12**), and isoterpinolene (**15**), and *p*-mentha-3,8-diene (**20**), all of which have olefin

in their structure, can partake in coupling reactions as compound **1** does. As electrophiles, stable allylic carbocations (**14**, **16**, and **18**) derived from these monocyclic isomers were thought to play a pivotal role in the coupling reaction [38,39]. This type of coupling can occur from the beginning to the end of a reaction, particularly in a predominant coupling reaction that occurs after compound **1** is completely consumed. In Scheme 2, we suggest some possible dimeric structures (**PD2–4**), showing that the isomers react as nucleophiles and electrophiles (carbocations).

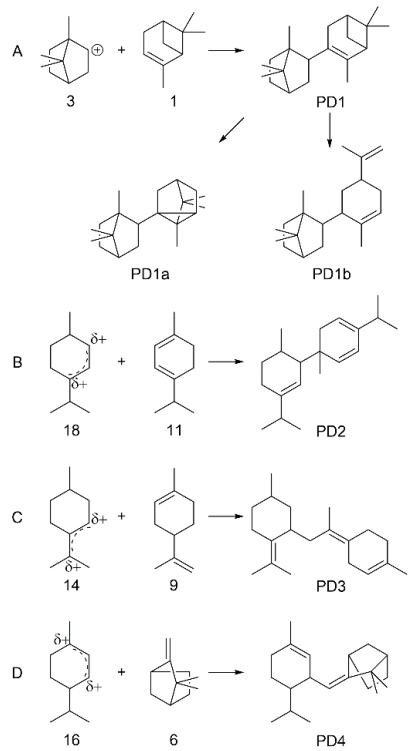

Scheme 2. Examples of possible dimeric products of the coupling reaction of α-pinene catalyzed using sulfated tin oxide: (**A**) coupling of bornanyl cation (**3**) and α-pinene (**1**) giving possible dimeric product (**PD1**) and its isomers (**PD1a–b**); (**B**) coupling of allylic carbocation III (**18**) and α-terpinene (**11**) giving **PD2**; (**C**) coupling of allylic carbocation I (**14**) and limonene (**9**) giving **PD3**; (**D**) coupling of allylic carbocation II (**16**) and camphene (**6**) giving **PD4**.

Although we are not sure whether camphene (**6**) reacts as a nucleophile or electrophile (as isocamphanyl cation (**5**)) during the coupling reaction, it is clear that compound **6** predominantly participates in a heterocoupling (Scheme 2, **PD4**) rather than a homocoupling reaction considering that a significant amount of compound **6** still remained after the reaction. This is in agreement with the results obtained using Al-incorporated MCM-41 [11]. Meylemans et al. asserted that this phenomenon is attributed to the low basicity of compound **6**, which causes poor interactions between the external olefin and the acid sites of the catalyst, thereby making the protonation of compound **6** difficult [7].

4. Conclusions

In summary, a sulfated tin(IV) oxide catalyst prepared using a facile procedure was applied to the partial coupling reaction of α-pinene to furnish a renewable and less viscous high-density fuel. To evaluate the catalytic activity of the catalyst, we considered the effect of the calcination temperature, reaction time, and reaction temperature, and attempted to rationalize the results using the catalyst characteristics. The catalyst calcination temperature had an enormous influence on the production of dimeric hydrocarbon products, while reaction times and temperatures exceeding 1 h and 100 °C affected the reaction to a lesser extent. The highest yield of dimeric products (49.6%) was obtained when the catalyst was calcined at 550 °C and the reaction was carried out at 120 °C for 4 h. Although

the yield was less than half, we think this value is enough to consider utilizing the reaction products as renewable fuels, because it is not known that the dimeric products alone have a low-temperature viscosity too high for use as a fuel in transportation engines. In other words, the mixture with the isomers of α-pinene can drag down the low-temperature viscosity to the range of transportation fuels. Finally, we described the possible mechanism of the coinstantaneous isomerization and coupling reaction of α-pinene owing to our catalyst acting as a Brønsted acid.

Supplementary Materials: The following are available online at http://www.mdpi.com/1996-1073/12/10/1905/s1, Figure S1: (a,b) Energy dispersive spectroscopy (EDS) spectra, (c,d) elemental quantitative data obtained from intact SnO_2 and SO_4^{2-}/SnO_2 and (e) higher resolution of elemental mapping image of SO_4^{2-}/SnO_2, Figure S2: TGA curves of intact SnO_2 (black line) and SO_4^{2-}/SnO_2 (red dashed line), Figure S3: The yields of the monomeric products along the reaction time at (a) 100 °C and (b) 110 °C, Figure S4: General chromatogram of dimeric products extracted from GC/FID result.

Author Contributions: Conceptualization, S.-M.C. and D.-S.L.; Data curation, S.-M.C., C.-Y.H. and B.K.; Formal analysis, S.-M.C., C.-Y.H. and B.K.; Methodology, S.-M.C. and D.-S.L.; Supervision, I.-G.C.; Writing—original draft, S.-M.C., S.-Y.P. and J.-H.C.; Writing—review & editing, C.-Y.H.

Funding: This study was supported by Mid-career Researcher Program in Basic Research of National Research Foundation of Korea grant funded by the Korea government (MSIP) (NRF-2016R1A2B4014222).

Conflicts of Interest: The authors declare no conflict of interest.

References

1. Gscheidmeier, M.; Fleig, H. Turpentines. In *Ullmann's Encyclopedia of Industrial Chemistry*; BASF Aktiengesellschaft: Ludwigshafen, Germany, 2012.
2. Yumrutaş, R.; Alma, M.H.; Özcan, H.; Kaşka, Ö. Investigation of Purified Sulfate Turpentine on Engine Performance and Exhaust Emission. *Fuel* **2008**, *87*, 252–259. [CrossRef]
3. Arpa, O.; Yumrutas, R.; Alma, M. Effects of Turpentine and Gasoline-Like Fuel Obtained from Waste Lubrication Oil on Engine Performance and Exhaust Emission. *Energy* **2010**, *35*, 3603–3613. [CrossRef]
4. Anand, B.P.; Saravanan, C.; Srinivasan, C.A. Performance and Exhaust Emission of Turpentine Oil Powered Direct Injection Diesel Engine. *Renew. Energy* **2010**, *35*, 1179–1184. [CrossRef]
5. Dubey, P.; Gupta, R. Influences of Dual Bio-Fuel (Jatropha Biodiesel and Turpentine Oil) on Single Cylinder Variable Compression Ratio Diesel Engine. *Renew. Energy* **2018**, *115*, 1294–1302.
6. Harvey, B.G.; Wright, M.E.; Quintana, R.L. High-Density Renewable Fuels Based on the Selective Dimerization of Pinenes. *Energy Fuels* **2009**, *24*, 267–273. [CrossRef]
7. Meylemans, H.A.; Quintana, R.L.; Harvey, B.G. Efficient Conversion of Pure and Mixed Terpene Feedstocks to High Density Fuels. *Fuel* **2012**, *97*, 560–568.
8. Jung, J.K.; Lee, Y.; Choi, J.-W.; Jae, J.; Ha, J.-M.; Suh, D.J.; Choi, J.; Lee, K.-Y. Production of High-Energy-Density Fuels by Catalytic β-Pinene Dimerization: Effects of the Catalyst Surface Acidity and Pore Width on Selective Dimer Production. *Energy Convers. Manag.* **2016**, *116*, 72–79. [CrossRef]
9. Meylemans, H.A.; Baldwin, L.C.; Harvey, B.G. Low-Temperature Properties of Renewable High-Density Fuel Blends. *Energy Fuels* **2013**, *27*, 883–888. [CrossRef]
10. Cho, S.-M.; Kim, J.-H.; Kim, S.-H.; Park, S.-Y.; Kim, J.-C.; Choi, I.-G. A Comparative Study on the Fuel Properties of Biodiesel from Woody Essential Oil Depending on Terpene Composition. *Fuel* **2018**, *218*, 375–384. [CrossRef]
11. Zou, J.J.; Chang, N.; Zhang, X.; Wang, L. Isomerization and Dimerization of Pinene using Al-Incorporated MCM-41 Mesoporous Materials. *ChemCatChem* **2012**, *4*, 1289–1297. [CrossRef]
12. Nie, G.; Zou, J.-J.; Feng, R.; Zhang, X.; Wang, L. HPW/MCM-41 Catalyzed Isomerization and Dimerization of Pure Pinene and Crude Turpentine. *Catal. Today* **2014**, *234*, 271–277. [CrossRef]
13. Zhang, S.; Xu, C.; Zhai, G.; Zhao, M.; Xian, M.; Jia, Y.; Yu, Z.; Liu, F.; Jian, F.; Sun, W. Bifunctional Catalyst Pd–Al-MCM-41 for Efficient Dimerization–Hydrogenation of β-Pinene in One Pot. *RSC Adv.* **2017**, *7*, 47539–47546. [CrossRef]
14. Andrea Merino, N.; Cecilia Avila, M.; Alejandra Comelli, N.; Natalia Ponzi, E.; Isabel Ponzi, M. Dimerization of α-Pinene, Using Phosphotungstic Acid Supported on SiO2 as Catalyst. *Curr. Catal.* **2014**, *3*, 240–243. [CrossRef]

15. Dabbawala, A.A.; Mishra, D.K.; Hwang, J.-S. Sulfated Tin Oxide as an Efficient Solid Acid Catalyst for Liquid Phase Selective Dehydration of Sorbitol to Isosorbide. *Catal. Commun.* **2013**, *42*, 1–5. [CrossRef]
16. Suzuki, T.; Yokoi, T.; Otomo, R.; Kondo, J.N.; Tatsumi, T. Dehydration of Xylose Over Sulfated Tin Oxide Catalyst: Influences of the Preparation Conditions on the Structural Properties and Catalytic Performance. *Appl. Catal. A Gen.* **2011**, *408*, 117–124. [CrossRef]
17. Moreno, J.; Jaimes, R.; Gómez, R.; Niño-Gómez, M. Evaluation of Sulfated Tin Oxides in the Esterification Reaction of Free Fatty Acids. *Catal. Today* **2011**, *172*, 34–40. [CrossRef]
18. Ahmed, A.I.; El-Hakam, S.; Khder, A.; El-Yazeed, W.A. Nanostructure Sulfated Tin Oxide as an Efficient Catalyst for the Preparation of 7-Hydroxy-4-Methyl Coumarin by Pechmann Condensation Reaction. *J. Mol. Catal. A Chem.* **2013**, *366*, 99–108. [CrossRef]
19. Bhure, M.H.; Kumar, I.; Natu, A.D.; Rode, C.V. Facile and Highly Selective Deprotection of Tert-Butyldimethyl Silyl Ethers Using Sulfated SnO2 as a Solid Catalyst. *Synth. Commun.* **2008**, *38*, 346–353. [CrossRef]
20. Gutierrez-Baez, R.; Toledo-Antonio, J.; Cortes-Jacome, M.; Sebastian, P.; Vázquez, A. Effects of the SO4 Groups on the Textural Properties and Local Order Deformation of SnO2 Rutile Structure. *Langmuir* **2004**, *20*, 4265–4271. [CrossRef]
21. Khder, A.; El-Sharkawy, E.; El-Hakam, S.; Ahmed, A. Surface Characterization and Catalytic Activity of Sulfated Tin Oxide Catalyst. *Catal. Commun.* **2008**, *9*, 769–777. [CrossRef]
22. Qi, X.; Watanabe, M.; Aida, T.M.; Smith, R.L., Jr. Sulfated Zirconia as a Solid Acid Catalyst for the Dehydration of Fructose to 5-Hydroxymethylfurfural. *Catal. Commun.* **2009**, *10*, 1771–1775. [CrossRef]
23. Trickett, C.A.; Popp, T.M.O.; Su, J.; Yan, C.; Weisberg, J.; Huq, A.; Urban, P.; Jiang, J.; Kalmutzki, M.J.; Liu, Q. Identification of the Strong Brønsted Acid Site in a Metal–Organic Framework Solid Acid Catalyst. *Nat. Chem.* **2019**, *11*, 170–176. [CrossRef] [PubMed]
24. Kassaye, S.; Pagar, C.; Pant, K.K.; Jain, S.; Gupta, R. Depolymerization of Microcrystalline Cellulose to Value Added Chemicals Using Sulfate Ion Promoted Zirconia Catalyst. *Bioresour. Technol.* **2016**, *220*, 394–400. [CrossRef] [PubMed]
25. Qiu, L.; Wang, Y.; Pang, D.; Ouyang, F.; Zhang, C. SO42−–Mn–Co–Ce Supported on TiO2/SiO2 with High Sulfur Durability for Low-Temperature SCR of NO with NH3. *Catal. Commun.* **2016**, *78*, 22–25. [CrossRef]
26. Saravanan, K.; Park, K.S.; Jeon, S.; Bae, J.W. Aqueous Phase Synthesis of 5-Hydroxymethylfurfural from Glucose over Large Pore Mesoporous Zirconium Phosphates: Effect of Calcination Temperature. *ACS Omega* **2018**, *3*, 808–820. [CrossRef]
27. Zhang, L.; Zou, W.; Ma, K.; Cao, Y.; Xiong, Y.; Wu, S.; Tang, C.; Gao, F.; Dong, L. Sulfated Temperature Effects on the Catalytic Activity of CeO2 in NH3-Selective Catalytic Reduction Conditions. *J. Phys. Chem. C* **2015**, *119*, 1155–1163. [CrossRef]
28. Yadav, M.K.; Chudasama, C.D.; Jasra, R.V. Isomerisation of α-Pinene Using Modified Montmorillonite Clays. *J. Mol. Catal. A Chem.* **2004**, *216*, 51–59. [CrossRef]
29. Kitano, T.; Okazaki, S.; Shishido, T.; Teramura, K.; Tanaka, T. Brønsted Acid Generation of Alumina-Supported Molybdenum Oxide Calcined at High Temperatures: Characterization by Acid-Catalyzed Reactions and Spectroscopic Methods. *J. Mol. Catal. A Chem.* **2013**, *371*, 21–28. [CrossRef]
30. Da Silva Rocha, K.A.; Robles-Dutenhefner, P.A.; Kozhevnikov, I.V.; Gusevskaya, E.V. Phosphotungstic Heteropoly Acid as Efficient Heterogeneous Catalyst for Solvent-Free Isomerization of α-Pinene and Longifolene. *Appl. Catal. A Gen.* **2009**, *352*, 188–192. [CrossRef]
31. Wang, J.; Hua, W.; Yue, Y.; Gao, Z. MSU-S Mesoporous Materials: An Efficient Catalyst for Isomerization of α-Pinene. *Bioresour. Technol.* **2010**, *101*, 7224–7230. [CrossRef]
32. Akgül, M.; Özyağcı, B.; Karabakan, A. Evaluation of Fe-And Cr-Containing Clinoptilolite Catalysts for the Production of Camphene from α-Pinene. *J. Ind. Eng. Chem.* **2013**, *19*, 240–249. [CrossRef]
33. Comelli, N.A.; Ponzi, E.N.; Ponzi, M.I. α-Pinene Isomerization to Camphene: Effect of Thermal Treatment on Sulfated Zirconia. *Chem. Eng. J.* **2006**, *117*, 93–99. [CrossRef]
34. Comelli, N.A.; Ponzi, E.N.; Ponzi, M.I. Isomerization of α-Pinene, Limonene, α-Terpinene, and Terpinolene on Sulfated Zirconia. *J. Am. Oil Chem. Soc.* **2005**, *82*, 531–535. [CrossRef]
35. Wróblewska, A.; Miądlicki, P.; Makuch, E. The Isomerization of α-Pinene over the Ti-SBA-15 Catalyst—The Influence of Catalyst Content and Temperature. *React. Kinet. Mech. Catal.* **2016**, *119*, 641–654. [CrossRef]

36. Yamamoto, T.; Matsuyama, T.; Tanaka, T.; Funabiki, T.; Yoshida, S. Generation of Acid Sites on Silica-Supported Rare Earth Oxide Catalysts: Structural Characterization and Catalysis for α-Pinene Isomerization. *Phys. Chem. Chem. Phys.* **1999**, *1*, 2841–2849. [CrossRef]
37. Lopes, C.; Lourenco, J.; Pereira, C.; Marcelo-Curto, M. Aromatization of Limonene with Zeolites Y. In *Natural Products in the New Millennium: Prospects and Industrial Application*; Springer: Berlin, Germany, 2002; pp. 429–436.
38. Salacinski, E.J. *Acid-Catalyzed Isomerization of the p-Menthadienes*; The University of Arizona: Tucson, AZ, USA, 1966.
39. McCormick, J.; Barton, D.L. Studies in 85% H3PO4—II: On the Role of the α-Terpinyl Cation in Cyclic Monoterpene Genesis. *Tetrahedron* **1978**, *34*, 325–330. [CrossRef]
40. Behr, A.; Wintzer, A. Hydroaminomethylation of the Renewable Limonene with Ammonia in an Aqueous Biphasic Solvent System. *Chem. Eng. Technol.* **2015**, *38*, 2299–2304. [CrossRef]
41. Al-Wadaani, F.; Kozhevnikova, E.F.; Kozhevnikov, I.V. Zn (II)–Cr (III) Mixed Oxide as Efficient Bifunctional Catalyst for Dehydroisomerisation of α-Pinene to P-Cymene. *Appl. Catal. A Gen.* **2009**, *363*, 153–156. [CrossRef]
42. Zhao, C.; Gan, W.; Fan, X.; Cai, Z.; Dyson, P.J.; Kou, Y. Aqueous-Phase Biphasic Dehydroaromatization of Bio-Derived Limonene into P-Cymene by Soluble Pd Nanocluster Catalysts. *J. Catal.* **2008**, *254*, 244–250. [CrossRef]
43. Golets, M.; Ajaikumar, S.; Mohln, M.; Wärnå, J.; Rakesh, S.; Mikkola, J.-P. Continuous Production of the Renewable ϱ-Cymene from α-Pinene. *J. Catal.* **2013**, *307*, 305–315. [CrossRef]
44. Linnekoski, J.A.; Asikainen, M.; Heikkinen, H.; Kaila, R.K.; Räsänen, J.; Laitinen, A.; Harlin, A. Production of P-Cymene from Crude Sulphate Turpentine with Commercial Zeolite Catalyst Using a Continuous Fixed Bed Reactor. *Org. Process Res. Dev.* **2014**, *18*, 1468–1475. [CrossRef]
45. Martin-Luengo, M.; Yates, M.; Rojo, E.S.; Arribas, D.H.; Aguilar, D.; Hitzky, E.R. Sustainable P-Cymene and Hydrogen from Limonene. *Appl. Catal. A Gen.* **2010**, *387*, 141–146. [CrossRef]
46. Arias-Ugarte, R.; Wekesa, F.S.; Schunemann, S.; Findlater, M. Iron (III)-Catalyzed Dimerization of Cycloolefins: Synthesis of High-Density Fuel Candidates. *Energy Fuels* **2015**, *29*, 8162–8167. [CrossRef]
47. Fernandes, C.; Catrinescu, C.; Castilho, P.; Russo, P.; Carrott, M.; Breen, C. Catalytic Conversion of Limonene over ACID ACTIVATED SERRA de Dentro (SD) Bentonite. *Appl. Catal. A Gen.* **2007**, *318*, 108–120. [CrossRef]

© 2019 by the authors. Licensee MDPI, Basel, Switzerland. This article is an open access article distributed under the terms and conditions of the Creative Commons Attribution (CC BY) license (http://creativecommons.org/licenses/by/4.0/).